DOI:
10.1093/hmg/ddx431

Document Version
Peer reviewed version

Myostatin inhibition using mRK35 produces skeletal muscle growth and tubular aggregate formation in wild type and Tg*ACTA1*^{D286G} nemaline myopathy mice

Jennifer A Tinklenberg[1], Emily M Siebers[1], Margaret J Beatka[1], Hui Meng[1], Lin Yang[2], Zizhao Zhang[2], Jacob A Ross[3], Julien Ochala[3], Carl Morris[4], Jane Owens[4], Nigel G Laing[5,6], Kristen J Nowak[6,7], and Michael W Lawlor[1*]

[1] Division of Pediatric Pathology, Department of Pathology and Laboratory Medicine and Neuroscience Research Center, Medical College of Wisconsin, Milwaukee, WI, USA

[2] Department of Biomedical Engineering, University of Florida, Gainesville, FL, USA

[3] School of Basic and Medical Biosciences, Faculty of Life Sciences and Medicine, King's College London, London, United Kingdom

[4] Pfizer Inc., Cambridge, MA, USA

[5] Centre for Medical Research, The University of Western Australia, Perth, Western Australia, Australia

[6] Harry Perkins Institute of Medical Research, Nedlands, Western Australia, Australia

[7] School of Biomedical Sciences, Faculty of Health and Medical Sciences, The University of Western Australia, Perth, Western Australia, Australia

Address for correspondence:

Michael W. Lawlor, MD, PhD

8701 Watertown Plank Rd

TBRC Building, Room C4490

Milwaukee, WI, 53226, USA

Tel: 414-955-2959

Fax: 414-266-2779

Email: mlawlor@mcw.edu

Abstract

Nemaline myopathy (NM) is a heterogeneous congenital skeletal muscle disease with cytoplasmic rod-like structures (nemaline bodies) in muscle tissue. While weakness in NM is related to contractile abnormalities, myofiber smallness is an additional abnormality in NM that may be treatable. We evaluated the effects of mRK35 (a myostatin inhibitor developed by Pfizer) treatment in the Tg*ACTA1*^{D286G} mouse model of NM. mRK35 induced skeletal muscle growth that led to significant increases in animal bodyweight, forelimb grip strength and muscle fiber force, although it should be noted that animal weight and forelimb grip strength in untreated Tg*ACTA1*^{D286G} mice was not different from controls. Treatment was also associated with an increase in the number of tubular aggregates found in skeletal muscle. These findings suggest that myostatin inhibition may be useful in promoting muscle growth and strength in *Acta1*-mutant muscle, while also further establishing the relationship between low levels of myostatin and tubular aggregate formation.

Introduction

Nemaline myopathies (NM) display a diverse range of clinical phenotypes(1) associated with mutations in at least 12 genes (*ACTA1, NEB, TPM3, TPM2, TNNT1, CFL2, KBTBD13, KLHL40, KLHL41, LMOD3, MYPN and MYO18B*)(2-9). All NM cases display nemaline rods upon skeletal muscle biopsy, which are aggregates of alpha-actinin and other sarcomeric proteins(10). The abundance, size and distribution of the nemaline rods does not correlate well with disease severity(2). While a variety of primary contractile abnormalities have been identified in NM patients and mouse models (11-18), myofiber smallness is another, more nonspecific pathological feature seen in many NM cases(19). As myofiber smallness (or insufficient numbers of sarcomeres in parallel) may contribute to skeletal muscle weakness in NM, we hypothesized that induction of myofiber hypertrophy would be of symptomatic benefit in murine models of NM.

We have previously used myostatin inhibition to pharmacologically induce myofiber hypertrophy in mice(20-22). Myostatin binds to (and signals through) the activin type IIB receptor (ActRIIB), which downregulates several key processes related to myofiber hypertrophy and activates the TGF-β pathway, thereby preventing progression through the cell cycle (23, 24). Nonfunctional decoys of ActRIIB can be used to inhibit this negative regulator of myofiber size leading to myofiber hypertrophy. In our prior work, we used ActRIIB-mFc, a soluble activin type IIB receptor with a murine Fc, to induce myofiber hypertrophy in wild type (WT) mice, in two murine models of X-linked myotubular myopathy (XLMTM)(20, 21), and in the KI.*Acta1*^{H40Y} mouse model of NM(22). While a dramatic and positive impact on skeletal muscle growth and function was observed in WT mice in all of these studies, the functional impact of

hypertrophy on XLMTM muscle was dramatically limited, possibly by the abnormalities of excitation-contraction coupling (ECC) that are also encountered in this disease (25-27). As deficiencies of ECC have not been observed in NM mice (11-15) or patients (16-18), this disease may be a more appropriate target in which to test myostatin inhibition therapy. In our recent studies, a trial of ActRIIB-mFc in the KI.*Acta1*^{H40Y} mouse model of NM, increased lifespan but did not impact other measures of muscle strength(22). Unfortunately, this study did not give a clear indication of whether myostatin inhibition would be useful in NM patients, particularly since the male KI.*Acta1*^{H40Y} mice often died from a disease complication (bladder outlet obstruction) that is not observed in human NM patients(10).

The current study assesses the effects of myostatin inhibition in a different NM mouse model (Tg*ACTA1*^{D286G}) using a second-generation myostatin inhibitor (anti-myostatin antibody, mRK35, Pfizer). mRK35 is a murine anti-myostatin antibody that binds to myostatin and GDF-11 with high affinity, without interfering with other ligands that signal through the ActRIIB receptors. In doing so, this antibody prevents myostatin binding to ActRIIB receptors thereby inhibiting downstream signaling to increase skeletal muscle mass and tetanic force (28) (29). To test the impact of mRK35 treatment in NM, Tg*ACTA1*^{D286G} and age matched WT C57Bl/6J (WT C57) mice were injected once per week with 10 mg/kg mRK35 until 6 months of age. Tg*ACTA1*^{D286G} mice treated with mRK35 showed an overall increase in bodyweight, skeletal muscle mass, myofiber size, forelimb grip strength and extensor digitorum longus (EDL) muscle fiber force. These findings illustrate the potential of myostatin inhibition to promote potentially useful muscle growth in the context of Acta1 mutations, although it should be noted that forelimb grip strength is not abnormally low in untreated Tg*ACTA1*^{D286G} mice. Additionally,

while increased numbers of tubular aggregate structures have been reported in Tg*ACTA1*^{D286G} mice (30), treatment with mRK35 produced an additional increase in their number. The mechanism responsible for tubular aggregate formation is unclear, but the formation of these structures did not appear to prevent treatment-related strength increases in these mice. Expression analysis of proteins associated with tubular aggregate formation detected treatment-associated trends towards an increase in SERCA1 in both mRK35-treated WT and Tg*ACTA1*^{D286G} mice. Overall, our results demonstrate the capacity for mRK35 to increase skeletal muscle strength in the Tg*ACTA1*^{D286G} mouse model of NM, although our results should be interpreted cautiously as several disease-associated phenotypes did not improve with mRK35 treatment.

Results

Animal Weight Studies

Vehicle-treated Tg*ACTA1*^{D286G} mice became distinguishable from vehicle-treated WT mice by 5 weeks of life (WOL) ($p<0.0332$, Figure 1A). At 6 WOL, WT mice treated with mRK35 began to show significant body weight gains compared to vehicle- treated WT mice (25.7g vs 23.3g, $p<0.0332$). mRK35-treated Tg*ACTA1*^{D286G} mice first showed significant body weight increases over vehicle-treated Tg*ACTA1*^{D286G} mice at 8 WOL (25.1g vs 22.4g, $p<0.0332$). These significant body weight increases then persisted throughout the course of the study.

Upon dissection of animals at 6 months of life, major skeletal muscles were harvested and weighed. Muscles of vehicle-treated Tg*ACTA1*^{D286G} mice that weighed significantly less than vehicle-treated WT mice included the diaphragm (79.3mg vs 103.67mg, $p<0.05$), triceps (112.06mg vs. 123.89mg, $p<0.05$), quadriceps (187.00mg vs 211.53mg, $p<0.05$), and gastrocnemii (125.33mg vs. 168.78mg, $p<0.05$) (Figure 1B). Treatment with mRK35 significantly increased the weights of triceps, quadriceps, and gastrocnemii in both WT and Tg*ACTA1*^{D286G} mice ($p<0.05$ for each; Figure 1B). Weight changes in the EDL muscle will be described below in the context of physiological testing.

Behavioral Studies

Forelimb grip strength, rotarod, running wheel, antigravity hanging performance, open field activity, and treadmill performance were used to evaluate skeletal muscle weakness and stamina. As forelimb grip strength provides a measure of "burst strength" that might be impacted by larger skeletal muscles, it was a particularly interesting endpoint in this study (Figure 1C).

Vehicle-treated Tg*ACTA1*^{D286G} mice did not have grip strength deficits in comparison to vehicle-treated WT mice. WT mice treated with mRK35 demonstrated greater grip strength than vehicle-treated WT mice starting at 9 WOL ($p<0.0332$). A similar treatment induced increase in grip strength was observed in mRK35-treated Tg*ACTA1*^{D286G} mice starting at 7 WOL ($p<0.0021$). Differences between groups fluctuated over the course of the 6 month study but ultimately persisted until termination (C57/VEH:C57/mRK35 $p<0.0002$; C57/VEH:D286G/mRK35 $p<0.0021$; D286G/VEH:D286G/mRK35 $p<0.0002$).

Other behavioral assays did not demonstrate changes due to mRK35 treatment, although deficits in specific assays (including running wheel and rotarod) were observed that confirm the disease phenotype originally reported in Tg*ACTA1*^{D286G} mice(14). Differences between voluntary locomotion in the open field test were significant when the animals were 1 month old (C57/VEH:D286G/VEH $p<0.0002$; C57/VEH:D286G/mRK35 $p<0.0001$), but were diminished by 3 months old and absent by 6 months of age (data not shown). As previously described (22, 30) the rotarod and voluntary running wheel assays distinguished WT from Tg*ACTA1*^{D286G} mice, but performance on these assays did not improve with mRK35 treatment. For the rotarod analyses, the vehicle-treated WT mice remained on the rod significantly longer than both the vehicle- and mRK35-treated Tg*ACTA1*^{D286G} mice ($p<0.0001$). However, mRK35-treated WT mice had poorer performance than untreated WT mice ($p<0.005$). No significant differences were observed between Tg*ACTA1*^{D286G} treatment groups. Over seven days of voluntary running wheel testing, Tg*ACTA1*^{D286G} mice had fewer wheel rotations than WT mice ($p<0.0021$, Figure 1D). Treatment with mRK35 did not affect voluntary running wheel performance of Tg*ACTA1*^{D286G} mice. This study also included assays that did not show significant differences

between groups with respect to either genotype or treatment, including antigravity hanging or treadmill performance assays (data not shown), but these assays were not completed on the full set of study animals.

Histopathological Studies

Histological evaluation of quadriceps and gastrocnemius muscles confirmed the previously reported abnormalities in Tg*ACTA1*^{D286G} mouse muscle, including the presence of decreased fiber size, internally-located nuclei, nemaline rods, and tubular aggregates (Figure 2). While myofiber size was decreased in vehicle-treated Tg*ACTA1*^{D286G} mice in comparison to vehicle-treated WT mice, mRK35 treatment increased myofiber size in mice of both genotypes (C57/VEH: 2805.4 ± 145.2 μm^2, C57/mRK: 3998.5 ± 159.8 μm^2, D286G/VEH: 2261.9 ± 99.4 μm^2, D286G/mRK: 3102.8 ± 141.1 μm^2, Figure 2B; C57/VEH:C57/mRK $p<0.0001$, C57/VEH: D286G/VEH $p<0.0332$ D286G/VEH: D286G/mRK $p<0.0002$). Estimations of the proportion of type 2b (fast, glycolytic) myofibers in the quadriceps muscle were made for a subset of study animals (n=6-9 per group). While there was extensive variation within groups, there was a minor skewing toward slightly increased proportions of type 2B fibers in C57 and Tg*ACTA1*^{D286G} mice treated with mRK35 (C57/VEH: 80.0+1.1%, C57/mRK: 86.9+2.3%, D286G/VEH: 67.5+5.4%, D286G/mRK: 75.8+3.0% type 2B fibers). There also was a trend toward a slightly smaller proportion of glycolytic fibers in the Tg*ACTA1*^{D286G} mice in comparison to the C57 animals. Prior work using the Tg*ACTA1*^{D286G} mouse has shown variable differences in the oxidative fiber subpopulations (type 1 and 2A) in some muscles, but variation in the type 2B fiber populations have not been reported(30).

As tubular aggregates and nemaline rods can both appear red on Gomori trichrome staining(31), the presence of tubular aggregates was confirmed by identifying dark blue intracytoplasmic inclusions on adenylate deaminase staining, and the presence of nemaline rods was confirmed by electron microscopy (Figure 2D). WT mouse muscles also displayed tubular aggregates in some myofibers (Figure 2A,C) in the absence of other pathological abnormalities. Muscles of mRK35-treatedWT mice had a trend toward increased percentages of fibers with tubular aggregates (C57/VEH: 28.1 ± 7.2 % of fibers, C57/mRK: 36.2 ± 7.2% of fibers, Figure 2C, p=ns) but were otherwise histologically normal. In contrast, there was a marked increase in tubular aggregates in the quadriceps muscles of Tg*ACTA1*^{D286G} mice following mRK35 treatment (D286G/VEH: 12.0 ± 3.8% of fibers, D286G/mRK: 50.7 ± 5.3% of fibers, Figure 2C, $p<0.0002$). Of note, there was also a significant increase in tubular aggregate formation in the triceps muscles of treated Tg*ACTA1*^{D286G} mice (D286G/VEH: 4.5 ± 0.6% of fibers, D286G/mRK: 17.1 ± 2.0% of fibers, data not shown, $p<0.0001$), confirming their presence in muscle groups that would be expected to have contributed to the increase in forelimb grip strength.

Physiological Studies

The functional impact of mRK35 treatment was further assessed via measurement of the absolute maximum isometric force of membrane-permeabilized single muscle fibers from the extensor digitorum longus (EDL) muscle. As comparisons of absolute and specific force can be impacted by muscle size and myofiber type changes, these features were assessed and compared across groups. The EDL muscle displayed a trend toward higher weights in both WT and Tg*ACTA1*^{D286G} mice after mRK35 treatment, but this did not reach statistical significance

(C57/vehicle = 10.04±0.58mg, C57/mRK35 = 14.62±0.47mg, D286G/vehicle = 9.77±0.48mg, D286G/mRK35 = 12.55±0.42mg, p = ns, N= 23-26 muscles per group) (Figure 3A). Histological evaluation of myofiber types in the EDL muscle showed similar proportions of slow and fast fibers in each treatment group. ATPase stains at pH 9.4 and immunostaining for myosin type 2B identified between 0-2 slow myofibers in each muscle, corresponding to a fairly uniform type 2B fiber proportion of 99-100% in the EDL irrespective of genotype or treatment (Figure 3B).

With respect to the functional characteristics of the EDL muscle, myofibers from vehicle-treated Tg*ACTA1*^{D286G} mice displayed a significant decrease in absolute maximum isometric force in comparison to myofibers from vehicle-treated WT mice, (C57/VEH: 359.3 ± 33.01 μN, D286G/VEH: 223.3 ± 22.2 μN, Figure 3C, p=0.0013). This is in accordance with our previously published data (32) (33). Treatment with mRK35 significantly increased absolute force in treated mice of both genotypes (C57/VEH: 359.3 ± 33.01 μN, C57/mRK: 512.9 ± 31.1 μN, p=0.0023; D286G/VEH: 223.3 ± 22.2 μN, D286G/mRK: 327.6 ± 25.68 μN, p=0.0041). Similarly, Tg*ACTA1*^{D286G} mice display significantly lower specific force compared to WT mice, regardless of treatment (C57/VEH: 135.9 ± 10.3.5 kPavs. D286G/VEH: 106.7 ± 7.445 kPa, p=0.0252; WT-mRK vs. D286G-mRK, Figure 3D, p=0.0027). However, mRK35 did not have any significant effect on specific force, which is consistent with a gain in force due to increased myofiber size rather than intrinsic contractile function(34-36). Thus, our findings indicate that treatment with mRK35 increases absolute maximum isometric force in WT and Tg*ACTA1*^{D286G} mice due to an increase in the amount of muscle available for contraction.

Hypertrophic Pathway Studies

The activation of hypertrophic pathways in WT and Tg*ACTA1*^{D286G} mice was investigated using western blots to measure protein expression. Many, phosphorylated and non-phosphorylated constituents of the Akt signaling pathway, including AKT, pAKT, P70/S6K, p-P70/S6K, p-rps6, ActRIIB, myostatin, and MTOR did not show significant differences with respect to genotype or treatment group (Figure 4). However, expression of rpS6 proteins was significantly greater in mRK35-treated WT mice than vehicle-treated WT mice (C57/VEH: 0.7049 ± 0.1476, C57/mRK: 1.286 ± 0.1739, Figure 4, p=0.0436). Levels of p-eEF2k in mRK35-treated WT mice were significantly greater than in mRK35-treated Tg*ACTA1*^{D286G} mice (C57/mRK: 0.03752 ± 0.004144, D286G/mRK: 0.01597 ± 0.004281, Figure 4, p=0.0111). Additionally, p-4EBP1 levels in mRK35-treated Tg*ACTA1*^{D286G} mice were significantly lower than both mRK35-treated WT mice and vehicle-treated Tg*ACTA1*^{D286G} mice (C57/mRK: 0.2029 ± 0.02263, D286G/VEH:0.1568 ± 0.02761, D286G/mRK: 0.06154 ± 0.01771, Figure 4, p= 0.0027 and 0.0272, respectively).

Composition of Tubular Aggregates

Expression of proteins related to tubular aggregate development (either known components of tubular aggregates or protein products of genes associated with tubular aggregate myopathies) was evaluated in WT and Tg*ACTA1*^{D286G} mice using western blot analysis. No significant differences in ORAI1, CASQ, Serca1, Dpagt1, calreticulin, or Stim1 were observed between any groups (Figure 5). mRK35 had no significant effect on tubular aggregate protein expression.

Discussion

In this study, we further examined the usefulness of myostatin inhibition therapy for NM using mRK35, a second-generation myostatin antibody, in the Tg*ACTA1*^{D286G} NM mouse model. We found that administration of mRK35 increased bodyweight, skeletal muscle mass, myofiber size and force, and forelimb grip strength, but also increased the formation of tubular aggregate structures in Tg*ACTA1*^{D286G} mice. While the results should be interpreted cautiously due to the lack of forelimb grip strength weakness in untreated Tg*ACTA1*^{D286G} mice, these findings support a role for increasing myofiber size as a means for improving skeletal muscle strength in at least some NM patients. As this benefit has been variable in our two studies of myostatin inhibition using two different *ACTA1*-NM models (described below), further study is required to predict the usefulness of these agents in human NM patients.

We have previously used ActRIIB-mFc (Acceleron Pharma), a first-generation myostatin inhibitor that acts as an ActRIIB receptor decoy, as our myostatin inhibition strategy in two studies of XLMTM(20, 21) and one study of NM(22) using mouse models. These studies established a significant capacity of ActRIIB-mFc to increase skeletal muscle size and strength in WT mice based on the inhibition of signaling through ActRIIB by myostatin or other ligands of this receptor. In this current study, we evaluated the therapeutic benefit of pharmacologically induced myofiber hypertrophy using an anti-myostatin antibody called mRK35 (developed by Pfizer, Inc). mRK35 was designed to selectively inhibit myostatin/GDF-11 signaling without affecting signaling by other ActRIIB and BMP receptor ligands (29) to provide a potentially more favorable safety profile compare to that reported with an ActRIIB antagonist (37). The present study establishes the capacity of mRK35 to increase skeletal muscle size and strength in WT mice, similar to the observed effects of ActRIIB-mFc treatment in our prior studies (20-22).

Furthermore, mRK35 significantly and persistently improved absolute myofiber force in the EDL and forelimb grip strength in Tg*ACTA1*^{D286G} mice, exceeding the benefits of myostatin inhibition that we observed in our prior studies of XLMTM mice or the KI.*Acta1*^{H40Y} mouse. With respect to their mechanism of action, mRK35 inhibits only myostatin and GDF-11 signaling whereas ActRIIB-mFc inhibits signaling induced by a panel of TGFb family members. Differences in these therapeutic candidates are unlikely to explain the observed dissimilarity in therapeutic efficacy between the two NM mouse models. It is instead more likely that the structural or functional derangement produced by the *Acta1* H40Y point mutation is less amenable to correction by the addition of skeletal muscle mass, whereas the *Acta1* D286G mutation is more amenable to correction using this strategy. However, as myofiber hypertrophy induced by cross-breeding KI.*Acta1*^{H40Y} mice with mice overexpressing FHL1 and IGF-1 did improve strength in KI.*Acta1*^{H40Y} mice(13), it is also possible that hypertrophy could be more broadly beneficial in NM if different pathways were used or the intervention occurred earlier in development.

It is important to note that the functional increases observed following mRK35 treatment of Tg*ACTA1*^{D286G} mice were restricted to forelimb grip strength and the absolute maximum isometric force of membrane-permeabilized single muscle fibers, and that some phenotypes associated with weakness in this model (running wheel performance and rotarod performance) did not improve with treatment. The increases in forelimb grip strength demonstrate that it is possible to increase strength in Tg*ACTA1*^{D286G} muscle using myostatin inhibition, and this assay has been highly useful in documenting treatment-related strength increases in control mice in our other myostatin inhibition studies(20, 22, 38) . As this phenotype is not abnormally weak in

untreated Tg*ACTA1*^{D286G} mice, however, it should be considered an "increase in strength" rather than an "improvement of a disease phenotype". With respect to the absolute force measurements in the EDL, however, one can observe a phenotype where tissue from Tg*ACTA1*^{D286G} mice display significant weakness in the untreated state and demonstrate an improvement in the context of mRK35 treatment. These differences are not apparent when the data are expressed as specific force (which normalizes data according to muscle size), which is most consistent with a treatment benefit that is solely explained by an increase in muscle fiber size. With respect to the lack of treatment-related improvement in rotarod and running wheel performance following mRK35 treatment, it is possible that these phenotypes are not well-suited to demonstrate improvements following myofiber growth, as no treatment-related benefits using these tests were observed in our wild type mice. In our prior studies of wild type mice, the forelimb grip strength test correlated well with myofiber hypertrophy, but other behavioral assays (antigravity hanging and open field activity, for instance) either remained unchanged or worsened with anti-myostatin therapy(20, 22). To our knowledge, running wheel and rotarod performance have not been studied elsewhere in control or diseased mice, but our data suggest that they may not be ideal assays for the detection of hypertrophy-related increases in strength.

Tubular aggregates are inclusions comprised of densely packed tubules that are thought to originate from the sarcoplasmic reticulum, SR (39). Several SR-associated proteins are highly expressed in tubular aggregates including sarcoplasmic endoplasmic reticulum Ca^{2+} ATPase 1 (SERCA1), calsequestrin, sarcalumenin, and RyR1(40). While tubular aggregates are observed in non-diseased, inbred male mice in association with increasing age(40, 41), very high levels of tubular aggregate formation have been observed in a variety of skeletal muscle diseases known

collectively as tubular aggregate myopathy (TAM), and mutations in *STIM1* and *ORAI1*, genes that encode proteins involved in calcium regulation, are associated with the development of TAM(42, 43). Due to the involvement of multiple proteins and genes related to calcium signaling, it is now believed that calcium dyshomeostasis drives the formation of tubular aggregates(44). Therefore, we investigated the expression of proteins involved in calcium regulation. We did not find any significant differences in the expression of proteins related to tubular aggregate formation, indicating that none of these proteins are reliable markers for the detection of tubular aggregates. These findings are curious considering the increased number of tubular aggregates seen upon microscopic evaluation. Perhaps tubular aggregate formation occurs from a redistribution of these proteins rather than differences in protein expression levels, which would not be detected with a western blot assay. Additionally, it should be noted that tubular aggregates appear in the skeletal muscles of old male mice in almost all mouse strains (41), and this study evaluated treatment efficacy in male mice only. It is unknown whether myostatin inhibition affects tubular aggregate formation in female mice.

In comparing this study of mRK35 treatment in Tg*ACTA1*^{D286G} mice to our prior studies using ActRIIB-mFc in WT, XLMTM, and KI.*Acta1*^{H40Y} mice, it is also noteworthy that we did not encounter tubular aggregates in our studies using ActRIIB-mFc. The present study identified a treatment-associated increase in fibers containing tubular aggregates in Tg*ACTA1*^{D286G} mice, but not WT mice (Figure 2). Our prior studies included mice of the C57/BL6 background(21) and mice at 6 months of age(21, 22), so mouse background strain and age does not explain the increase in tubular aggregates in Tg*ACTA1*^{D286G} mice. It is possible that formation of tubular aggregates is an effect of mRK35 treatment in Tg*ACTA1*^{D286G} mice that may not be produced

when using ActRIIB-mFc. As tubular aggregates have also been reported in myostatin-knockout mice(45), the formation of tubular aggregates may be a consequence of a specific deficiency in myostatin. Additional experiments in larger numbers of WT mice may be useful in more clearly defining the promotion of tubular aggregate formation by various myostatin inhibitors.

Western blots were conducted to determine the effect of the Tg*ACTA1*^{D286G} mutation on hypertrophy signaling and the degree to which mRK35 therapy altered signaling in these pathways. Treatment with mRK35 increased total rpS6 levels in WT mice. However, no significant differences in the levels of proteins involved in hypertrophic pathway signaling between vehicle-treated WT and Tg*ACTA1*^{D286G} mice were observed. As in our prior studies(21, 22), it is possible that hypertrophic signaling events were missed at earlier time points and that myofiber growth had plateaued by 6 months of life. Abnormalities of hypertrophyd signaling in our prior work were clearest in the context of a lack of response to treatment(22), whereas the Tg*ACTA1*^{D286G} muscles appeared to be fully responsive to treatment in this study and hypertrophic pathway activation may not be any different from WT muscle.

Interestingly, mRK35 did not affect myostatin receptor abundance. Our current findings are consistent with our previous report that demonstrated myostatin inhibition using ActRIIB-mFc resulted in muscle hypertrophy without affecting myostatin receptor expression in the knockout mouse model of myotubular myopathy, although it should once again be noted that ActRIIB-mFc inhibits myostatin less specifically than mRK35(38). In a previous study using the KI.*Acta1*^{H40Y} mouse model, abnormalities in myostatin expression were observed in untreated mice, and myostatin inhibition with ActRIIB-mFc upregulated myostatin receptor expression in

WT mice and decreased expression in KI.*Acta1*^{H40Y} mice (22). These findings indicate the method of myostatin inhibition (antimyostatin-antibody vs. receptor decoy) may have different effects on myostatin receptor expression and that mouse strain and disease model affect receptor expression following myostatin inhibition. As noted above, it is also possible that differences in myostatin and its receptor would be present at an earlier stage of treatment, but tissue was not taken at earlier timepoints to address this possibility.

In summary, we show that administration of an anti-myostatin antibody (mRK35) which binds to myostatin and inhibits its signaling activity, increased muscle growth in Tg*ACTA1*^{D286G} mice, which resulted in significant increases in animal body weight, skeletal muscle weights, myofiber size and force, and forelimb grip strength. Additionally, mRK35-treated Tg*ACTA1*^{D286G} mice had increased numbers of tubular aggregates in skeletal muscle. Collectively, our findings indicate that a more selective myostatin inhibitor may be a therapeutic intervention to increase strength in at least a subset of NM, while also further establishing the relationship between low levels of myostatin and tubular aggregate formation.

Materials and Methods

Live Animal Studies

All studies were performed with approval from the IACUC at The Medical College of Wisconsin. Genotyping of the Tg*ACTA1*^{D286G} mice was performed as previously described(13). Male Tg*ACTA1*^{D286G} mice were homozygous for the *ACTA1* mutation (30). Male C57Bl/6J male mice were used as the wild type (WT) control. Beginning at 14-17 days of postnatal life, all mice were given intraperitoneal injections of mRK35 (Pfizer, New York, NY) once per week at a dose of 10 mg/kg, or an equivalent volume of Dulbecco's phosphate buffered saline (PBS, the vehicle used with mRK35)(20). Mice were weighed five days per week during the treatment period, beginning when the first injection was given. Once the mice were weaned at three weeks of age, forelimb grip strength was measured weekly using a grip strength meter (Columbus Instruments, Columbus, OH, USA)(22). Antigravity hanging performance, open field and treadmill analysis were also performed as previously described(22). As a terminal physiological test, mice were placed on a rotarod (IITC Life Sciences, Woodland Hills, CA) and then with voluntary running wheels (Coulbourn Instruments, Whitehall, PA) (14, 22) and monitored for wheel count activity for seven days. Mice were then euthanized for tissue collection at 6 months of age.

Pathological Evaluation and Tissue Collection

CO_2 euthanasia was used followed by cervical dislocation. Skin was removed and photographs were taken to assess skeletal muscle bulk. Internal organs, brain, and a variety of skeletal muscles (quadriceps, gastrocnemius, triceps, soleus, extensor digitorum longus, diaphragm) were removed. The skeletal muscles were weighed, and frozen in liquid nitrogen-cooled isopentane and then stored at -80^{o}C, whilst the organs were placed in zinc-buffered formalin.

Muscle Histology

Quadriceps, gastrocnemius, and EDL muscle samples were cross sectioned at 8 μm, mounted on slides and stained with hematoxylin and eosin (H&E), Gomori trichrome, ATPase at pH 9.4, or adenylate deaminase (31) for evaluation using an Olympus BX53 microscope with an Olympus DP72 camera and cellSens Standard software (Olympus, Center Valley, PA, USA). Frozen 8 μm quadriceps cross sections were also double-stained with rabbit anti-dystrophin antibodies (ab15277, Abcam, Cambridge, MA, 1:100) and mouse monoclonal antibodies against myosin heavy chain type 2b (clone BF-F3, Developmental Studies Hybridoma Bank (DSHB), Iowa City, IA, 1:50) to determine myofiber size and type. Secondary antibodies used were Alexa Fluor® 488 conjugated anti-mouse IgM (Sigma Aldrich, St. Louis, MO, 1:400) and Alexa Fluor® 594-conjugated anti-rabbit IgG (Molecular Probes, Carlsbad, CA, 1:200).

Fiber size was determined in quadriceps muscle samples through measurements of myofiber cross sectional area (20, 46). As in our recent studies(22), quantitation was performed by evaluating the type 2b myosin positive (glycolytic) and type 2b myosin negative (oxidative) populations on a whole slide scan of one quadriceps muscle from 7 vehicle-treated WT mice, 6 mRK35-treated WT mice, 6 vehicle-treated Tg*ACTA1*^{D286G} mice, and 6 mRK35-treated Tg*ACTA1*^{D286G}. MinFeret diameter was evaluated using an automated technique developed by Dr. Lin Yang, as we have previously reported (20, 21).

Single Fiber Functional Studies

For myofiber force measurements, we treated EDL muscles immediately after dissection with

skinning solution (relaxing solution containing glycerol; 50:50 v/v) for 24 hours at 4°C, after which they were transferred to -20°C (47). Single muscle fibers were dissected following the same procedure as above. They were then individually attached between connectors leading to a force transducer (model 400A; Aurora Scientific) and a lever arm system (model 308B; Aurora Scientific). Sarcomere length was set to ≈2.50 μm (known to be optimal for force measurement) and the temperature to 15°C (33, 48, 49). The absolute maximal isometric force generation was calculated as the difference between the total tension in the activating solution and the resting tension measured in the same fiber while in the relaxing solution. Specific force was defined as absolute force divided by the fiber cross-sectional area (CSA, estimated from the width and depth, assuming an elliptical circumference (33, 48, 49)). Relaxing and activating solutions contained 4 mM Mg-ATP, 1 mM free Mg^{2+}, 20 mM imidazole, 7 mM EGTA, 14.5 mM creatine phosphate, and KCl to adjust the ionic strength to 180 mM and pH to 7.0. The concentrations of free Ca^{2+} were $10^{-9.00}$ M (relaxing solution) and $10^{-4.50}$ M (activating solution).

Organ Histology

Formalin-fixed organs from 5 animals per treatment group were paraffin embedded at the Children's Hospital of Wisconsin Research Institute Histology Core, as previously described(50, 51) and stained using H&E. Organ histology was reviewed by a board certified anatomic- and neuro-pathologist to assess for a full range of possible disease- or treatment-related structural abnormalities.

Western Blots

Whole gastrocnemius muscles were sliced into 8 μm sections using a cryostat and homogenized with lysing buffer (EMD Millipore, Temecula, CA) containing protease inhibitor (Roche, Basel, Switzerland) and phosphatase inhibitor (Roche Basel, Switzerland). Western blot procedures were performed as previously described(21, 22, 52). Transferred proteins were probed with antibodies against various antigens. Antibodies obtained from Cell Signaling Technologies include those for the following antigens: Akt (4691), phospho-Akt (Ser473; 4060), p70-S6K (2708), phospho-p70-S6K (Thr421/Ser424; 9204), S6 ribosomal protein (2217), phospho-S6 ribosomal protein (Ser240/244; 5364), phospho-eEF2k (Ser366; 3691), phospho-4E-BP1 (Thr37/46; 2855), and MTOR (2983). Antibodies obtained from Invitrogen included those recognizing the following antigens: androgen receptor (AR441), calreticulin (PA3-900), calsequestrin (VIIID12, MA3-913), ORAI1 (6D11A11), Rbfox1 (PA5-29074), and STIM1 (CDN3H4). Antibodies recognizing the following antigens that were obtained from Abcam include: ActRIIB (ab76940), Gfpt1 (ab125069), and Dpagt1 (ab117459). Other antibodies used for western blot studies recognize: ankyrin (MAB1683, EMD Millipore), GAPDH (G8795, Sigma Aldrich), myostatin (MAB788, R&D Systems, Minneapolis, MN), obscurin (ABT160, EMD Millipore), and SERCA1 ATPase (MA3-911, Pierce, Rockford, IL). Antibodies were visualized using the appropriate species-specific chemiluminescent HRP antibody detection reagent (Bio-Rad Laboratories, Hercules, CA). Adequacy of transfer was determined by Ponceau S staining. Quantification of protein levels normalized to GAPDH was performed with Image Lab Software (Bio-Rad Laboratories). Four mice per treatment group were used for analysis.

Statistical Analysis

ANOVAs were performed using Prism 7.0 software (Graphpad, Inc.) on animal bodyweight, forelimb grip strength, open field activity, antigravity hanging performance, voluntary running wheel, and treadmill performance, and average myofiber size. Tukey post-tests were performed on all behavioral measures. For statistical analysis of western blot data, t-tests were used to compare protein expression between different genotypes or treatments.

Acknowledgements

We thank Dr. Gianina Ravenscroft for helpful discussions and scientific advice. Behavioral testing was performed at the Neuroscience Research Center's Behavioral Core Facility at the Medical College of Wisconsin, which is funded by the Research and Education Initiative Fund, a component of the Advancing a Healthier Wisconsin Endowment at the Medical College of Wisconsin. Histology and imaging work was performed (in part) using the Histology and Imaging Core Facilities at the Children's Hospital of Wisconsin Research Institute.

This work was supported by funding from the National Institutes of Health (K08 AR059750). NL was funded by an Australian National Health and Medical Research Council Fellowship (APP1117510), KN by an Australian Research Council Future Fellowship (FT100100734) and JO by a grant from the Medical Research Council UK (MR/N002768/1).

Conflict of Interest Statement

Dr. MW Lawlor is a member of advisory boards for Audentes Therapeutics, and has been supported by sponsored research agreements by Audentes Therapeutics, Solid Biosciences, and Ichorion Therapeutics. He is a scientific collaborator with Acceleron Pharma and Pfizer Inc. He was also a consultant for Sarepta Therapeutics at the time that some of this work was performed. Dr. C Morris is a prior employee of Pfizer Inc and a current employee of Solid Biosciences. Dr. J Owens is a current employee of Pfizer Inc.

References

1 North, K.N., Laing, N.G. and Wallgren-Pettersson, C. (1997) Nemaline myopathy: current concepts. The ENMC International Consortium and Nemaline Myopathy. *Journal of medical genetics*, **34**, 705-713.

2 Wallgren-Pettersson, C., Sewry, C.A., Nowak, K.J. and Laing, N.G. (2011) Nemaline myopathies. *Seminars in pediatric neurology*, **18**, 230-238.

3 Gupta, V.A., Ravenscroft, G., Shaheen, R., Todd, E.J., Swanson, L.C., Shiina, M., Ogata, K., Hsu, C., Clarke, N.F., Darras, B.T. *et al.* (2013) Identification of KLHL41 Mutations Implicates BTB-Kelch-Mediated Ubiquitination as an Alternate Pathway to Myofibrillar Disruption in Nemaline Myopathy. *American journal of human genetics*, **93**, 1108-1117.

4 Ravenscroft, G., Miyatake, S., Lehtokari, V.L., Todd, E.J., Vornanen, P., Yau, K.S., Hayashi, Y.K., Miyake, N., Tsurusaki, Y., Doi, H. *et al.* (2013) Mutations in KLHL40 are a frequent cause of severe autosomal-recessive nemaline myopathy. *American journal of human genetics*, **93**, 6-18.

5 Yuen, M., Sandaradura, S.A., Dowling, J.J., Kostyukova, A.S., Moroz, N., Quinlan, K.G., Lehtokari, V.L., Ravenscroft, G., Todd, E.J., Ceyhan-Birsoy, O. *et al.* (2014) Leiomodin-3 dysfunction results in thin filament disorganization and nemaline myopathy. *J. Clin. Invest.*, in press.

6 Miyatake, S., Mitsuhashi, S., Hayashi, Y.K., Purevjav, E., Nishikawa, A., Koshimizu, E., Suzuki, M., Yatabe, K., Tanaka, Y., Ogata, K. *et al.* (2017) Biallelic Mutations in MYPN, Encoding Myopalladin, Are Associated with Childhood-Onset, Slowly Progressive Nemaline Myopathy. *American journal of human genetics*, **100**, 169-178.

7 Lornage, X., Malfatti, E., Cheraud, C., Schneider, R., Biancalana, V., Cuisset, J.M., Garibaldi, M., Eymard, B., Fardeau, M., Boland, A. *et al.* (2017) Recessive MYPN mutations cause cap myopathy with occasional nemaline rods. *Ann. Neurol.*, **81**, 467-473.

8 Malfatti, E., Bohm, J., Lacene, E., Beuvin, M., Romero, N.B. and Laporte, J. (2015) A Premature Stop Codon in MYO18B is Associated with Severe Nemaline Myopathy with Cardiomyopathy. *J. Neuromuscul. Dis.*, **2**, 219-227.

9 Alazami, A.M., Kentab, A.Y., Faqeih, E., Mohamed, J.Y., Alkhalidi, H., Hijazi, H. and Alkuraya, F.S. (2015) A novel syndrome of Klippel-Feil anomaly, myopathy, and characteristic facies is linked to a null mutation in MYO18B. *J. Med. Genet.*, **52**, 400-404.

10 Dubowitz, V., Sewry, C. and Oldfors, A. (2013) Dubowitz, V., Sewry, C. and Oldfors, A. (eds.), In *Muscle Biopsy: A Practical Approach*. Saunders Elsevier, in press., pp. 358-405.

11 Chandra, M., Mamidi, R., Ford, S., Hidalgo, C., Witt, C., Ottenheijm, C., Labeit, S. and Granzier, H. (2009) Nebulin alters cross-bridge cycling kinetics and increases thin filament activation: a novel mechanism for increasing tension and reducing tension cost. *J. Biol. Chem.*, **284**, 30889-30896.

12 de Haan, A., van der Vliet, M.R., Gommans, I.M., Hardeman, E.C. and van Engelen, B.G. (2002) Skeletal muscle of mice with a mutation in slow alpha-tropomyosin is weaker at lower lengths. *Neuromuscul. Disord.*, **12**, 952-957.

13 Nguyen, M.A., Joya, J.E., Kee, A.J., Domazetovska, A., Yang, N., Hook, J.W., Lemckert, F.A., Kettle, E., Valova, V.A., Robinson, P.J. *et al.* (2011) Hypertrophy and dietary tyrosine ameliorate the phenotypes of a mouse model of severe nemaline myopathy. *Brain*, **134**, 3516-3529.

14 Ravenscroft, G., Jackaman, C., Bringans, S., Papadimitriou, J.M., Griffiths, L.M., McNamara, E., Bakker, A.J., Davies, K.E., Laing, N.G. and Nowak, K.J. (2011) Mouse models of dominant ACTA1 disease recapitulate human disease and provide insight into therapies. *Brain*, **134**, 1101-1115.

15 Witt, C.C., Burkart, C., Labeit, D., McNabb, M., Wu, Y., Granzier, H. and Labeit, S. (2006) Nebulin regulates thin filament length, contractility, and Z-disk structure in vivo. *EMBO J*, **25**, 3843-3855.

16 Ottenheijm, C.A., Witt, C.C., Stienen, G.J., Labeit, S., Beggs, A.H. and Granzier, H. (2009) Thin filament length dysregulation contributes to muscle weakness in nemaline myopathy patients with nebulin deficiency. *Hum. Mol. Genet.*, **18**, 2359-2369.

17 Ottenheijm, C.A., Lawlor, M.W., Stienen, G.J., Granzier, H. and Beggs, A.H. (2011) Changes in cross-bridge cycling underlie muscle weakness in patients with tropomyosin 3-based myopathy. *Hum. Mol. Genet.*, **20**, 2015-2025.

18 Ottenheijm, C.A., Hooijman, P., DeChene, E.T., Stienen, G.J., Beggs, A.H. and Granzier, H. (2010) Altered myofilament function depresses force generation in patients with nebulin-based nemaline myopathy (NEM2). *J. Struct. Biol.*, **170**, 334-343.

19 Imoto, C. and Nonaka, I. (2001) The significance of type 1 fiber atrophy (hypotrophy) in childhood neuromuscular disorders. *Brain & development*, **23**, 298-302.

20 Lawlor, M.W., Read, B.P., Edelstein, R., Yang, N., Pierson, C.R., Stein, M.J., Wermer-Colan, A., Buj-Bello, A., Lachey, J.L., Seehra, J.S. *et al.* (2011) Inhibition of activin receptor type IIb increases strength and lifespan in myotubularin-deficient mice. *Am. J. Pathol.*, **178**, 784-793.

21 Lawlor, M.W., Viola, M.G., Meng, H., Edelstein, R.V., Liu, F., Yan, K., Luna, E.J., Lerch-Gaggl, A., Hoffmann, R.G., Pierson, C.R. *et al.* (2014) Differential Muscle Hypertrophy Is Associated with Satellite Cell Numbers and Akt Pathway Activation Following Activin Type IIB Receptor Inhibition in Mtm1 p.R69C Mice. *Am. J. Pathol.*, in press.

22 Tinklenberg, J., Meng, H., Yang, L., Liu, F., Hoffmann, R.G., Dasgupta, M., Allen, K.P., Beggs, A.H., Hardeman, E.C., Pearsall, R.S. *et al.* (2016) Treatment with ActRIIB-mFc Produces Myofiber Growth and Improves Lifespan in the Acta1 H40Y Murine Model of Nemaline Myopathy. *Am. J. Pathol.*, **186**, 1568-1581.

23 McCroskery, S., Thomas, M., Maxwell, L., Sharma, M. and Kambadur, R. (2003) Myostatin negatively regulates satellite cell activation and self-renewal. *J. Cell. Biol.*, **162**, 1135-1147.

24 Joulia-Ekaza, D. and Cabello, G. (2006) Myostatin regulation of muscle development: molecular basis, natural mutations, physiopathological aspects. *Exp. Cell. Res.*, **312**, 2401-2414.

25 Al-Qusairi, L., Weiss, N., Toussaint, A., Berbey, C., Messaddeq, N., Kretz, C., Sanoudou, D., Beggs, A.H., Allard, B., Mandel, J.L. *et al.* (2009) T-tubule disorganization and defective excitation-contraction coupling in muscle fibers lacking myotubularin lipid phosphatase. *Proc. Natl. Acad. Sci. U S A*, **106**, 18763-18768.

26 Dowling, J.J., Vreede, A.P., Low, S.E., Gibbs, E.M., Kuwada, J.Y., Bonnemann, C.G. and Feldman, E.L. (2009) Loss of myotubularin function results in T-tubule disorganization in zebrafish and human myotubular myopathy. *PLoS Genet.*, **5**, e1000372.

27 Lawlor, M.W., Armstrong, D., Viola, M.G., Widrick, J.J., Meng, H., Grange, R.W., Childers, M.K., Hsu, C.P., O'Callaghan, M., Pierson, C.R. *et al.* (2013) Enzyme replacement

therapy rescues weakness and improves muscle pathology in mice with X-linked myotubular myopathy. *Hum. Mol. Genet.*, **22**, 1525-1538.

28 Apgar, J.R., Mader, M., Agostinelli, R., Benard, S., Bialek, P., Johnson, M., Gao, Y., Krebs, M., Owens, J., Parris, K. *et al.* (2016) Beyond CDR-grafting: Structure-guided humanization of framework and CDR regions of an anti-myostatin antibody. *MAbs*, **8**, 1302-1318.

29 St Andre, M., Johnson, M., Bansal, P.N., Wellen, J., Robertson, A., Opsahl, A., Burch, P.M., Bialek, P., Morris, C. and Owens, J. (2017) A mouse anti-myostatin antibody increases muscle mass and improves muscle strength and contractility in the mdx mouse model of Duchenne muscular dystrophy and its humanized equivalent, domagrozumab (PF-06252616), increases muscle volume in cynomolgus monkeys. *Skelet. Muscle*, **7**, 25.

30 Ravenscroft, G., Jackaman, C., Sewry, C.A., McNamara, E., Squire, S.E., Potter, A.C., Papadimitriou, J., Griffiths, L.M., Bakker, A.J., Davies, K.E. *et al.* (2011) Actin nemaline myopathy mouse reproduces disease, suggests other actin disease phenotypes and provides cautionary note on muscle transgene expression. *PLoS ONE*, **6**, e28699.

31 (2013) Dubowitz, V., Sewry, C.A. and Oldfors, A. (eds.), In *Muscle Biopsy: A Practical Approach*. Saunders Elsevier, in press., pp. 16-27.

32 Ochala, J., Ravenscroft, G., McNamara, E., Nowak, K.J. and Iwamoto, H. (2015) X-ray recordings reveal how a human disease-linked skeletal muscle alpha-actin mutation leads to contractile dysfunction. *J. Struct. Biol.*, **192**, 331-335.

33 Ochala, J., Ravenscroft, G., Laing, N.G. and Nowak, K.J. (2012) Nemaline myopathy-related skeletal muscle alpha-actin (ACTA1) mutation, Asp286Gly, prevents proper strong myosin binding and triggers muscle weakness. *PLoS ONE*, **7**, e45923.

34 Bechir, N., Pecchi, E., Vilmen, C., Le Fur, Y., Amthor, H., Bernard, M., Bendahan, D. and Giannesini, B. (2016) ActRIIB blockade increases force-generating capacity and preserves energy supply in exercising mdx mouse muscle in vivo. *FASEB J*, **30**, 3551-3562.

35 Bogdanovich, S., Krag, T.O., Barton, E.R., Morris, L.D., Whittemore, L.A., Ahima, R.S. and Khurana, T.S. (2002) Functional improvement of dystrophic muscle by myostatin blockade. *Nature*, **420**, 418-421.

36 Pistilli, E.E., Bogdanovich, S., Goncalves, M.D., Ahima, R.S., Lachey, J., Seehra, J. and Khurana, T. (2011) Targeting the activin type IIB receptor to improve muscle mass and function in the mdx mouse model of Duchenne muscular dystrophy. *Am. J. Pathol.*, **178**, 1287-1297.

37 Campbell, C., McMillan, H.J., Mah, J.K., Tarnopolsky, M., Selby, K., McClure, T., Wilson, D.M., Sherman, M.L., Escolar, D. and Attie, K.M. (2017) Myostatin inhibitor ACE-031 treatment of ambulatory boys with Duchenne muscular dystrophy: Results of a randomized, placebo-controlled clinical trial. *Muscle Nerve*, **55**, 458-464.

38 Lawlor, M.W., Viola, M.G., Meng, H., Edelstein, R.V., Liu, F., Yan, K., Luna, E.J., Lerch-Gaggl, A., Hoffmann, R.G., Pierson, C.R. *et al.* (2014) Differential muscle hypertrophy is associated with satellite cell numbers and Akt pathway activation following activin type IIB receptor inhibition in Mtm1 p.R69C mice. *Am. J. Pathol.*, **184**, 1831-1842.

39 Liu, F., Mackey, A.L., Srikuea, R., Esser, K.A. and Yang, L. (2013) Automated image segmentation of haematoxylin and eosin stained skeletal muscle cross-sections. *Journal of microscopy*, **252**, 275-285.

40 Chevessier, F., Marty, I., Paturneau-Jouas, M., Hantai, D. and Verdiere-Sahuque, M. (2004) Tubular aggregates are from whole sarcoplasmic reticulum origin: alterations in calcium

binding protein expression in mouse skeletal muscle during aging. *Neuromuscul. Disord.*, **14**, 208-216.

41 Agbulut, O., Destombes, J., Thiesson, D. and Butler-Browne, G. (2000) Age-related appearance of tubular aggregates in the skeletal muscle of almost all male inbred mice. *Histochem. Cell. Biol.*, **114**, 477-481.

42 Bohm, J., Chevessier, F., Maues De Paula, A., Koch, C., Attarian, S., Feger, C., Hantai, D., Laforet, P., Ghorab, K., Vallat, J.M. *et al.* (2013) Constitutive activation of the calcium sensor STIM1 causes tubular-aggregate myopathy. *Am. J. Hum. Genet.*, **92**, 271-278.

43 Endo, Y., Noguchi, S., Hara, Y., Hayashi, Y.K., Motomura, K., Miyatake, S., Murakami, N., Tanaka, S., Yamashita, S., Kizu, R. *et al.* (2015) Dominant mutations in ORAI1 cause tubular aggregate myopathy with hypocalcemia via constitutive activation of store-operated Ca(2)(+) channels. *Hum. Mol. Genet.*, **24**, 637-648.

44 Lee, J.M. and Noguchi, S. (2016) Calcium Dyshomeostasis in Tubular Aggregate Myopathy. *Int. J. Mol. Sci.*, **17**.

45 Amthor, H., Macharia, R., Navarrete, R., Schuelke, M., Brown, S.C., Otto, A., Voit, T., Muntoni, F., Vrbova, G., Partridge, T. *et al.* (2007) Lack of myostatin results in excessive muscle growth but impaired force generation. *Proc. Natl. Acad. Sci. U S A*, **104**, 1835-1840.

46 Brooke, M.H. and Engel, W.K. (1969) The histographic analysis of human muscle biopsies with regard to fiber types. 4. Children's biopsies. *Neurology*, **19**, 591-605.

47 Frontera, W.R. and Larsson, L. (1997) Contractile studies of single human skeletal muscle fibers: a comparison of different muscles, permeabilization procedures, and storage techniques. *Muscle & nerve*, **20**, 948-952.

48 Lindqvist, J., Cheng, A.J., Renaud, G., Hardeman, E.C. and Ochala, J. (2013) Distinct underlying mechanisms of limb and respiratory muscle fiber weaknesses in nemaline myopathy. *J. Neuropathol. Exp. Neurol.*, **72**, 472-481.

49 Ochala, J., Iwamoto, H., Ravenscroft, G., Laing, N.G. and Nowak, K.J. (2013) Skeletal and cardiac alpha-actin isoforms differently modulate myosin cross-bridge formation and myofibre force production. *Hum. Mol. Gen.*, **22**, 4398-4404.

50 Kheir, J.N., Scharp, L.A., Borden, M.A., Swanson, E.J., Loxley, A., Reese, J.H., Black, K.J., Velazquez, L.A., Thomson, L.M., Walsh, B.K. *et al.* (2012) Oxygen gas-filled microparticles provide intravenous oxygen delivery. *Sci. Transl. Med.*, **4**, 140ra188.

51 Moghadaszadeh, B., Rider, B.E., Lawlor, M.W., Childers, M.K., Grange, R.W., Gupta, K., Boukedes, S.S., Owen, C.A. and Beggs, A.H. (2013) Selenoprotein N deficiency in mice is associated with abnormal lung development. *FASEB J*, **27**, 1585-1599.

52 Wattanasirichaigoon, D., Swoboda, K.J., Takada, F., Tong, H.Q., Lip, V., Iannaccone, S.T., Wallgren-Pettersson, C., Laing, N.G. and Beggs, A.H. (2002) Mutations of the slow muscle alpha-tropomyosin gene, TPM3, are a rare cause of nemaline myopathy. *Neurology*, **59**, 613-617.

Figure Legends

Figure 1. Behavioral impact of mRK35 treatment in WT and Tg*ACTA1*^{D286G} mice. (A) Total bodyweight of VEH- and mRK35-treated mice. Treatment of WT mice and Tg*ACTA1*^{D286G} with mRK35 produced significant increases in body mass. **(B)** Individual muscle weights (mg) from VEH- and mRK35-treated mice. Treatment of WT mice and Tg*ACTA1*^{D286G} with mRK35 produced significant increases in triceps, quadriceps, and gastrocnemius muscle weights. **(C)** Forelimb grip force of VEH- and mRK35-treated mice. Treatment of WT mice and Tg*ACTA1*^{D286G} with mRK35 produced significant increases in forelimb grip strength. **(D)** Running wheel testing identified clear differences between genotypes over 7 days of testing, but no impact of treatment in either WT or Tg*ACTA1*^{D286G} mice. Bars and asterisk denote significant (* $P \leq 0.05$, ** $P \leq 0.01$, *** $P \leq 0.001$, **** $P \leq 0.0001$) differences between treatment groups with relevant comparisons.

Figure 2. Pathological impact of mRK35 treatment in WT and Tg*ACTA1*^{D286G} mice. **(A)** Representative areas of transversely sectioned quadriceps muscle after sectioning and staining. Histology reveals decreased myofiber size in Tg*ACTA1*^{D286G} mice compared to WT controls. Cytoplasmic aggregates were observed on Gomori trichrome and adenylate deaminase staining, characteristic of tubular aggregates. **(B)** Histogram illustrating myofiber size in quadricep muscles of VEH- and mRK35-treated WT and Tg*ACTA1*^{D286G} mice. Treatment with mRK35 significantly increased myofiber size in WT and Tg*ACTA1*^{D286G} mice. **(C)** Histogram illustrating percent of quadriceps muscle cells containing tubular aggregates. Treatment with mRK35 markedly increases the percentage of fibers housing tubular aggregates in Tg*ACTA1*^{D286G} mice. **(D)** Electron microscopy images of tubular aggregates (yellow arrow) and

nemaline bodies (white arrow). Bars and asterisk denote significant (* $P \leq 0.05$, ** $P \leq 0.01$, *** $P \leq 0.001$, **** $P \leq 0.0001$) differences between treatment groups with relevant comparisons.

Figure 3. Fiber force measurements in the EDL muscle following mRK35 treatment in WT and Tg*ACTA1*^{D286G} mice. (A) Weights of EDL muscles in study animals (two muscles per animal). (B) Representative images using ATPase stains at pH 9.4 on the EDL muscle show glycolytic (type 2) fibers in dark brown and oxidative (type 1) fibers in light tan, with approximately 99-100% type 2 fibers observed in all samples evaluated (n=3 per group). **(C)** Absolute maximum isometric force (μN) of membrane-permeabilized single muscle fibers of the extensor digitorum longus determined by the difference between total tension in activating solution and resting tension. **(D)** Specific force (kPa) for muscles in **(C)**, calculated as absolute force divided by fiber cross-sectional area. Asterisks denote significant ($P < 0.05$) differences between treatment groups with relevant comparisons. Error bars indicate standard error of the mean (SEM).

Figure 4. Expression of proteins related to myofiber growth following mRK35 treatment in WT and Tg*ACTA1*^{D286G} mice. (A) Western blots reveal protein expression of growth-associated proteins in the gastrocnemius of individual WT or Tg*ACTA1*^{D286G} mice. **(B)** Quantified protein expression (normalized to GAPDH expression) for each growth-associated protein shown in **(A)**. Protein extracted from the gastrocnemius muscle of four 27-week old mice per treatment group was tested. Asterisks denote significant ($P < 0.05$) differences between treatment groups with

relevant comparisons. Error bars indicate SEM. ActRIIB, activin type IIB receptor; GAPDH, glyceraldenhyde-3-phophate dehydrogenase.

Figure 5. Expression of proteins related to tubular aggregates in vehicle- and MRK-treated mice. (A) Western blots reveal protein expression of tubular aggregate-associated proteins in the gastrocnemius of individual WT or Tg*ACTA1*^{D286G} mice. (**B)** Quantified protein expression (normalized to GAPDH expression) for each protein shown in **(A)**. Protein extracted from the gastrocnemius muscle of four 27-week old mice per treatment group was tested. Error bars indicated SEM. CASQ, calsequestrin; GAPDH, glyceraldenhyde-3-phophate dehydrogenase.

Abbreviations

ActRIIB: activin type IIB receptor

ECC: excitation-contraction coupling

GLM: generalized linear models

NM: nemaline myopathy

Ns: not significant

SEM: standard error of the mean

SERCA1: sarcoplasmic endoplasmic reticulum Ca^{2+} ATPase 1

SR: sarcoplasmic reticulum

TAM: tubular aggregate myopathy

WT: wild-type

XLMTM: X-linked myotubular myopathy

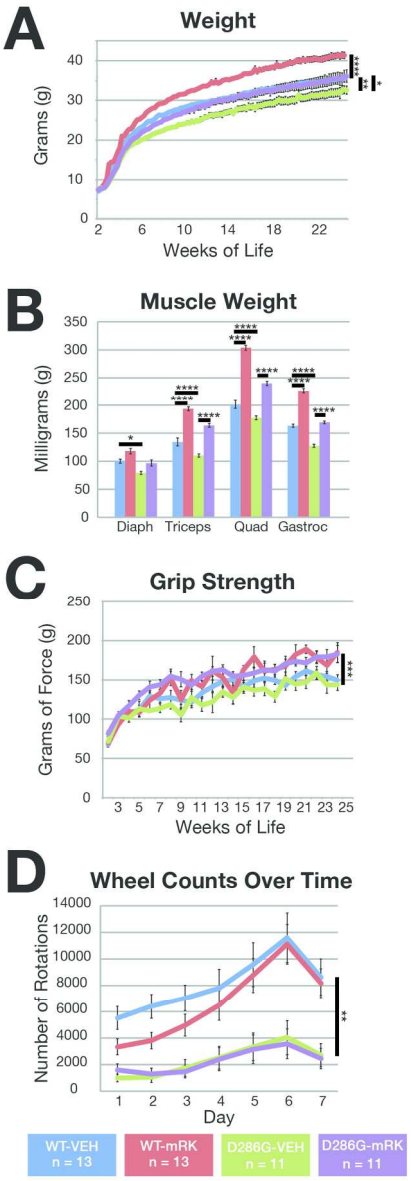

Figure 1. Behavioral impact of mRK35 treatment in WT and TgACTA1D286G mice. (A) Total bodyweight of VEH- and mRK35-treated mice. Treatment of WT mice and TgACTA1D286G with mRK35 produced significant increases in body mass. (B) Individual muscle weights (mg) from VEH- and mRK35-treated mice. Treatment of WT mice and TgACTA1D286G with mRK35 produced significant increases in triceps, quadriceps, and gastrocnemius muscle weights. (C) Forelimb grip force of VEH- and mRK35-treated mice. Treatment of WT mice and TgACTA1D286G with mRK35 produced significant increases in forelimb grip strength. (D) Running wheel testing identified clear differences between genotypes over 7 days of testing, but no impact of treatment in either WT or TgACTA1D286G mice. Bars and asterisk denote significant (* $P \leq 0.05$, ** $P \leq 0.01$, *** $P \leq 0.001$, **** $P \leq 0.0001$) differences between treatment groups with relevant comparisons.

86x211mm (300 x 300 DPI)

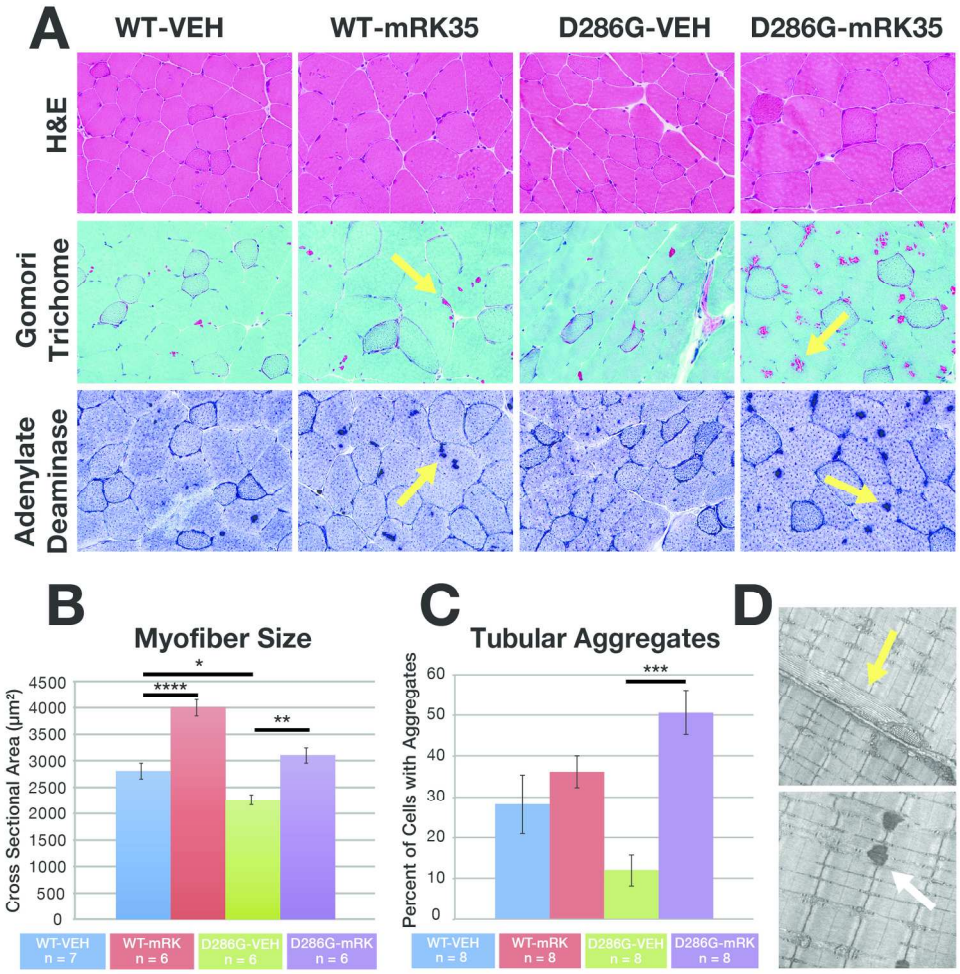

Figure 2. Pathological impact of mRK35 treatment in WT and TgACTA1D286G mice. (A) Representative areas of transversely sectioned quadriceps muscle after sectioning and staining. Histology reveals decreased myofiber size in TgACTA1D286G mice compared to WT controls. Cytoplasmic aggregates were observed on Gomori trichrome and adenylate deaminase staining, characteristic of tubular aggregates. (B) Histogram illustrating myofiber size in quadricep muscles of VEH- and mRK35-treated WT and TgACTA1D286G mice. Treatment with mRK35 significantly increased myofiber size in WT and TgACTA1D286G mice. (C) Histogram illustrating percent of quadriceps muscle cells containing tubular aggregates. Treatment with mRK35 markedly increases the percentage of fibers housing tubular aggregates in TgACTA1D286G mice. (D) Electron microscopy images of tubular aggregates (yellow arrow) and nemaline bodies (white arrow). Bars and asterisk denote significant (* $P \leq 0.05$, ** $P \leq 0.01$, *** $P \leq 0.001$, **** $P \leq 0.0001$) differences between treatment groups with relevant comparisons.

180x185mm (300 x 300 DPI)

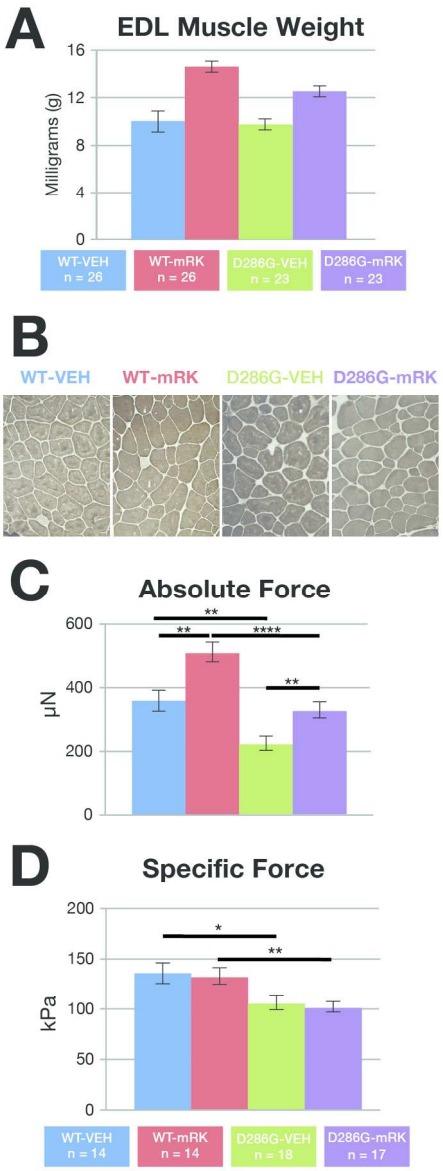

Figure 3. Fiber force measurements in the EDL muscle following mRK35 treatment in WT and TgACTA1D286G mice. (A) Weights of EDL muscles in study animals (two muscles per animal). (B) Representative images using ATPase stains at pH 9.4 on the EDL muscle show glycolytic (type 2) fibers in dark brown and oxidative (type 1) fibers in light tan, with approximately 99-100% type 2 fibers observed in all samples evaluated (n=3 per group). (C) Absolute maximum isometric force (µN) of membrane-permeabilized single muscle fibers of the extensor digitorum longus determined by the difference between total tension in activating solution and resting tension. (D) Specific force (kPa) for muscles in (C), calculated as absolute force divided by fiber cross-sectional area. Asterisks denote significant ($P < 0.05$) differences between treatment groups with relevant comparisons. Error bars indicate standard error of the mean (SEM).

86x220mm (300 x 300 DPI)

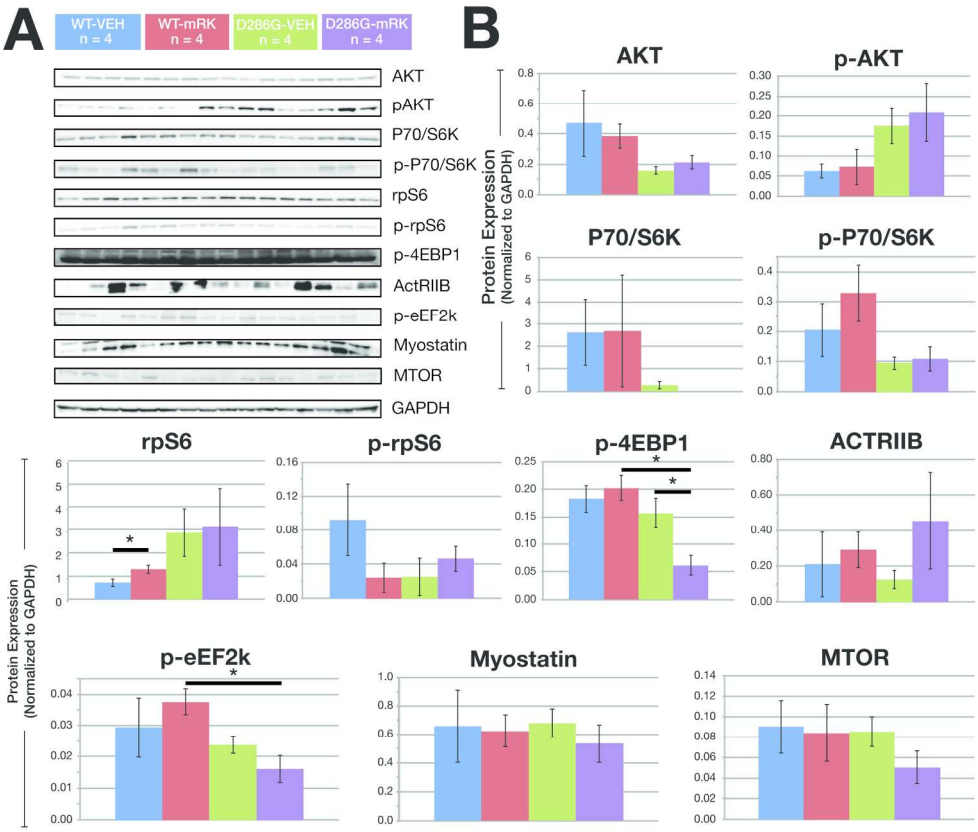

Figure 4. Expression of proteins related to myofiber growth following mRK35 treatment in WT and TgACTA1D286G mice. (A) Western blots reveal protein expression of growth-associated proteins in the gastrocnemius of individual WT or TgACTA1D286G mice. (B) Quantified protein expression (normalized to GAPDH expression) for each growth-associated protein shown in (A). Protein extracted from the gastrocnemius muscle of four 27-week old mice per treatment group was tested. Asterisks denote significant ($P < 0.05$) differences between treatment groups with relevant comparisons. Error bars indicate SEM. ActRIIB, activin type IIB receptor; GAPDH, glyceraldenhyde-3-phophate dehydrogenase.

180x151mm (300 x 300 DPI)

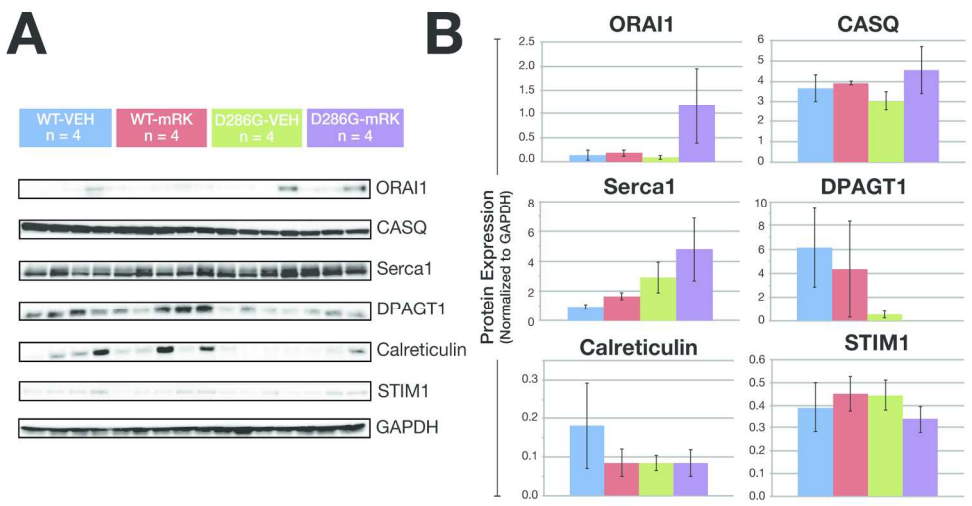

Figure 5. Expression of proteins related to tubular aggregates in vehicle- and MRK-treated mice. (A) Western blots reveal protein expression of tubular aggregate-associated proteins in the gastrocnemius of individual WT or TgACTA1D286G mice. (B) Quantified protein expression (normalized to GAPDH expression) for each protein shown in (A). Protein extracted from the gastrocnemius muscle of four 27-week old mice per treatment group was tested. Error bars indicated SEM. CASQ, calsequestrin; GAPDH, glyceraldenhyde-3-phophate dehydrogenase.

180x91mm (300 x 300 DPI)